Low-order stochastic model and "past-noise forecasting" of the Madden-Julian Oscillation

D. Kondrashov,[1] M. D. Chekroun,[1] A. W. Robertson,[2] and M. Ghil[1,3]

Received 9 July 2013; revised 18 September 2013; accepted 20 September 2013; published 10 October 2013.

[1] This paper presents a predictability study of the Madden-Julian Oscillation (MJO) that relies on combining empirical model reduction (EMR) with the "past-noise forecasting" (PNF) method. EMR is a data-driven methodology for constructing stochastic low-dimensional models that account for nonlinearity, seasonality and serial correlation in the estimated noise, while PNF constructs an ensemble of forecasts that accounts for interactions between (i) high-frequency variability (noise), estimated here by EMR, and (ii) the low-frequency mode of MJO, as captured by singular spectrum analysis (SSA). A key result is that—compared to an EMR ensemble driven by generic white noise—PNF is able to considerably improve prediction of MJO phase. When forecasts are initiated from weak MJO conditions, the useful skill is of up to 30 days. PNF also significantly improves MJO prediction skill for forecasts that start over the Indian Ocean. **Citation:** Kondrashov, D., M. D. Chekroun, A. W. Robertson, and M. Ghil (2013), Low-order stochastic model and "past-noise forecasting" of the Madden-Julian Oscillation, *Geophys. Res. Lett.*, *40*, 5305–5310, doi:10.1002/grl.50991.

1. Introduction

[2] The Madden-Julian Oscillation (MJO) is the dominant mode of intraseasonal variability across the global tropics. The MJO is a natural component of the coupled atmosphere-ocean system and it affects other important climate processes, in both the tropics and extratropics; these processes include the seasonal evolution of temperature and precipitation, tropical cyclone frequency, and weather extremes.

[3] In this paper, we built on the extensive studies to improve prediction of the daily indices of the Real-Time Multivariate MJO Index, known as RMM1 and RMM2 [*Wheeler and Hendon*, 2004]. These indices are dominated by intraseasonal fluctuations due to MJO variability in the 40–50 day band. The predictive statistical models used so far can be grouped roughly into (i) multiple lagged regression-based models [*Jiang et al.*, 2008; *Seo et al.*, 2009; *Maharaj and Wheeler*, 2005; *Kang and Kim*, 2010] and (ii) models based on advanced time series analysis, such as singular spectrum analysis (SSA) and wavelets [*Kang and Kim*, 2010], neural networks [*Love and Matthews*, 2009], and analogs [*Seo et al.*, 2009]. The useful predictive skill for the MJO of such empirical models is typically of about 15–20 days, and it is similar to the MJO forecast skill achieved by state-of-the-art dynamical models [*Vitart and Molteni*, 2010; *Zhang and van den Dool*, 2012; *Zhang et al.*, 2013].

[4] We propose here to bring to bear on empirical MJO prediction a combination of novel tools (i) for the construction of stochastic low-dimensional models (LDMs) and (ii) for the application of the LDMs so constructed to prediction. The LDM construction is carried out by data-driven empirical model reduction (EMR), which accounts for nonlinearity, seasonality, and serial correlation in the noise estimate [*Kravtsov et al.*, 2005, 2009]. The prediction method is the pathwise past-noise forecasting (PNF) method [*Checkroun et al.*, 2011a], which improves predictions by accounting for the modulation of high-frequency variability, or "noise," by the MJO's low-frequency mode (LFM), as captured by SSA.

[5] The understanding and reliable description of LFMs is of the essence for the prediction of the high amplitude but irregularly occurring events in the frequency bands of interest [*Ghil and Robertson*, 2002]. Furthermore, it is crucial to understand the interaction between LFMs and the higher-frequency variability [*Chekroun et al.*, 2011a].

[6] This interaction can be better understood in the framework of random dynamical systems (RDS) theory, in which the stochastic dynamics is studied pathwise—i.e., for individual realizations of the noise—rather than being merely sampled by an ensemble of forward trajectories that aim to approximate the system's probability density function (PDF) [*Chekroun et al.*, 2011b]. This pathwise view of the dynamics helps in applying inverse stochastic nonlinear models to prediction, since such an inverse model "lives" naturally on the estimated path of the noise, as derived from the data.

[7] So far, though, it was not clear how to derive such pathwise models. Most of the inherent difficulties have been overcome by using the EMR methodology [*Kravtsov et al.*, 2005, 2009] to yield nonlinear stochastic inverse models that successfully capture the LFMs of the climatic phenomena of interest [*Kondrashov et al.*, 2011, 2005], while also estimating the path of the noise.

[8] *Chekroun et al.* [2011a] extended the results of *Kondrashov et al.* [2005] beyond the sampled PDF approach and developed PNF as a general pathwise method for nonlinear stochastic systems that exhibit LFMs. This method exploits information on the estimated path on which the inverse stochastic model evolves, as well as on the interaction between the model's deterministic, nonlinear

Additional supporting information may be found in the online version of this article.

[1]Department of Atmospheric and Oceanic Sciences and Institute of Geophysics and Planetary Physics, University of California, Los Angeles, California, USA.
[2]International Research Institute for Climate and Society, Columbia University, Palisades, New York, USA.
[3]Laboratoire de Météorologie Dynamique, Geosciences Department, CNRS and IPSL, Ecole Normale Supérieure, Paris, France.

Corresponding author: D. Kondrashov, Department of Atmospheric and Oceanic Sciences, University of California, 405 Hilgard Ave., PO Box 951565, 7127 Math Sciences Bldg., Los Angeles, CA 90095-1565, USA. (dkondras@atmos.ucla.edu)

©2013. American Geophysical Union. All Rights Reserved.
0094-8276/13/10.1002/grl.50991

components and the stochastic ones. PNF has been shown to outperform classical ensemble prediction techniques on synthetic, model-generated data, as well as on observational data for El Niño–Southern Oscillation (ENSO) [*Chekroun et al.*, 2011a].

2. Methods

2.1. Empirical Model Reduction

[9] The EMR approach represents a generalization of linear inverse modeling (LIM) [*Penland and Sardeshmukh*, 1995]. As an operational prediction methodology, EMR constructs a low-order nonlinear system of prognostic equations driven by stochastic forcing; the method estimates the model's deterministic part, as well as the properties of the driving noise from the observations or from a more detailed model's simulation.

[10] EMR relies on multilevel polynomial inverse modeling: It thus allows (a) the model to be nonlinear and (b) the noise terms to be correlated in space and serially correlated in time [*Kravtsov et al.*, 2005]. Like other model-reduction methodologies, it adopts a stochastic approach to describe a system of coupled, slow-and-fast variables. *Kravstov et al.* [2009] reviewed EMR and its applications and compared it with other methodologies. They showed EMR to be particularly effective (1) when variability of the faster parts of the system is both modulated by and feeds back on the slower components of the system and (2) when there is no significant time scale separation between slow and fast variables.

[11] A multilevel EMR model can be formally written as the following set of $M+1$ vector equations:

$$\begin{aligned} \dot{\mathbf{x}} &= \mathbf{F} - \mathbf{A}\mathbf{x} + \mathbf{B}(\mathbf{x},\mathbf{x}) + \mathbf{r}_t^0, \\ \dot{\mathbf{r}}_t^{m-1} &= \mathbf{L}^{(m)}(\mathbf{x}, \mathbf{r}_t^0, \ldots, \mathbf{r}_t^{m-1}) + \mathbf{r}_t^m, \ 1 \le m \le M, \end{aligned} \tag{1}$$

Here $\mathbf{x} = (x_i; i = 1, \ldots, d)$ represents the resolved modes on the main level of the model, while $\mathbf{r}_t^m$ at additional levels accounts for unresolved modes, which at the last level are approximated as spatially correlated white noise $\mathbf{r}_t^M \approx \mathbf{\Sigma}\dot{\mathbf{W}}$.

[12] For our MJO application, $d = 2$ and x_1 and x_2 are the RMM1 and RMM2 indices. The terms $-\mathbf{A}\mathbf{x}$ and $\mathbf{B}(\mathbf{x},\mathbf{x})$ represent the linear dissipation and the quadratic self-interactions, respectively, while $\mathbf{F}$ accounts for the deterministic forcing [*Kondrashov et al.*, 2011]. Memory effects of the interactions between the resolved variables $\mathbf{x}$ and the unresolved $\mathbf{r}_t^m$ arise as convolution terms by integrating recursively the "matrioshka" of levels from the lowest level M to the main level [*Wouters and Lucarini*, 2013; D. Kondrashov et al., Data-driven reduction by multilayered stochastic models with energy-preserving nonlinearities, submitted to *Physica D-Nonlinear Phenomena*, 2013]. The coupling between the variable $\mathbf{r}_t^m$ and the variables $(\mathbf{x}, \mathbf{r}_t^0, \ldots, \mathbf{r}_t^{m-1})$ from the previous levels is modeled by rectangular matrices $\mathbf{L}^{(m)}$ of increasing size.

[13] When deriving a time-discrete formulation of equation (1), instantaneous tendencies $\delta\mathbf{x}/\delta t$ and $\delta\mathbf{r}_t^m/\delta t$ are computed numerically by Euler time differencing and are used to estimate by recursive least squares the coefficients $\mathbf{F}$, $\mathbf{A}$, $\mathbf{B}$, and $\mathbf{L}^{(m)}$, as well as computing the regression residuals $\mathbf{r}_t^{m+1}$, to be modeled at the next level. The procedure is stopped when the estimated $\xi_t \equiv \mathbf{r}_t^M$ has an autocorrelation that vanishes at unit lag and its spatial covariance matrix has converged to a constant matrix $\mathbf{\Sigma}$.

[14] Standard forecasting by EMR relies on forward integration of the model from a given initial state and driven at the last model level by a large ensemble of random realizations of the estimated noise $\mathbf{\Sigma}\dot{\mathbf{W}}$. ENSO real-time prediction by EMR [*Kondrashov et al.*, 2005] is highly competitive among other dynamical and statistical forecasts in the ENSO multimodel prediction plume of the International Research Institute for Climate and Society (IRI) at Columbia University, [*Barnston et al.*, 2012].

[15] For this study, we tested an energy-conserving EMR formulation to ensure that $\|x\| = \sum_{i=1}^{d} x_i^2 < \infty$ (see the supporting information). We have found that in the case of MJO, there was no noticeable difference in prediction skill between strictly energy-conserving EMR and its nonenergy conserving implementation.

2.2. Past-Noise Forecasting by EMR

[16] We start by building a nonlinear EMR model using past observations and we estimate the path of the "weather" noise ξ_t (see section 2.1) that drove this model over previous finite time windows. The PNF method is then applied in two steps. First, noise snippets—obtained as copies of this estimated path—are selected from past time intervals during which the LFM phase resembles that observed prior to a particular forecast. Second, these noise snippets—which have the same length as the forecast lead time—are used to drive the system into the future.

[17] We rely on SSA to identify a nearly periodic LFM in the (RMM1, RMM2) data set. SSA is a data adaptive, nonparametric method for spectral estimation that extends classic principal component analysis into the time lag domain [*Vautard and Ghil*, 1989]. In practice, the LFMs are described by the reconstructed components (RCs) given by SSA [*Ghil et al.*, 2002]. These RCs are then used for the noise snippet selection here, by finding in the past record analogs of the LFM that best match the LFM phase just preceding the start of the forecast. Such a conditioning of the noise forcing on the LFM phase improves forecast skill, and so-called linear pathwise response with respect to noise perturbations helps explain the PNF method's success [cf. *Chekroun et al.*, 2011a].

3. Results and Discussion

[18] We developed a quadratic EMR model with three levels (main plus two, i.e., $M = 2$ in section 2.1) to simulate and predict the (RMM1, RMM2) daily indices (RMM1–2 hereafter) for June 1974 to January 2009 (see http://cawcr.gov.au/staff/mwheeler/maproom/RMM/ for the data set). Following *Kondrashov et al.* [2005], we included the seasonal cycle effects into the forcing and the linear part, i.e., $\mathbf{F}$ and $\mathbf{A}$ in equation (1), on the model's main level.

[19] Figures 1a and 1b compare the autocorrelation functions (ACFs) of the RMM1–2 time series, EMR simulated versus observed, when using a large ensemble of EMR stochastic realizations. Figures 1a and 1b demonstrate that the EMR model captures very well the ACFs, and hence, the MJO power spectrum, as well as its 40–60 day LFM. We found that the use of $M > 1$ improves the EMR-MJO model's prediction skill at long lead times (not shown).

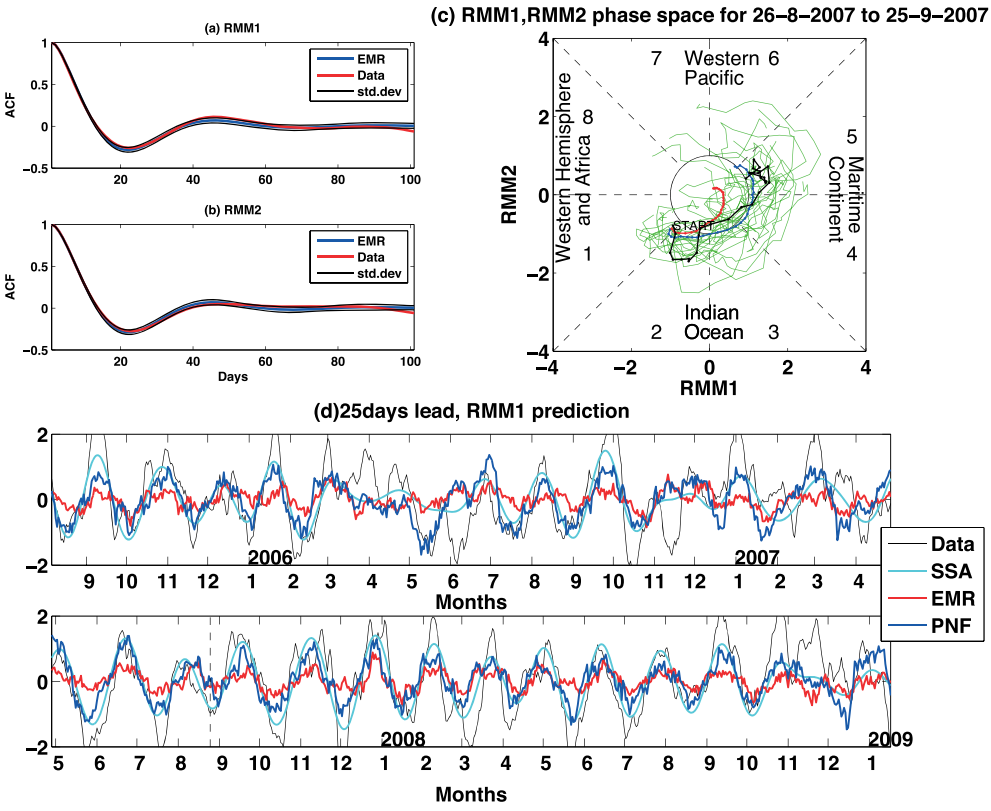


Figure 1. Comparison between the simulation and prediction capabilities of the EMR model with the PNF-modified version thereof. Autocorrelation functions (ACFs) of the (a) RMM1 and (b) RMM2 daily indices: observations—red, ensemble mean of the EMR simulations—blue, and standard deviation of the EMR ensemble—black. (c) Improved prediction of the observed RMM1-RMM2 indices (black) by PNF-based driving-noise selection: PNF ensemble mean (blue) versus EMR ensemble mean (red), and individual members of the PNF ensemble (green); the predictions in Figure 1c, out to 30 days, all start on 26 August 2007, namely, the date that is marked by the black dashed line in Figure 1. (d) PNF prediction in the time domain of RMM1 (black) at a 25 day lead is consistent with MJO's LFM, captured by SSA RCs 1–2 (cyan); x axis is time in calendar months within the validation interval of July 2005 to January 2009.

[20] The EMR model was trained on the June 1974 to July 2005 portion of the RMM1–2 record, and forecasts were validated for the independent time interval July 2005 to January 2009. In this study, we modified the noise snippet selection in the PNF procedure of *Chekroun et al.* [2011a] by adopting a suggestion of *Feliks et al.* [2010], namely, to determine an instantaneous phase $0 < \phi < 2\pi$ of narrowband LFM components via the Hilbert transform applied to the SSA reconstruction of the latter, i.e., to the leading RC pair of RMM1. This selection procedure results in a fixed size of 20 PNF ensemble members per t^*, where t^* is the forecast start time within the validation interval, compared to EMR ensemble driven by 200 independent realizations of white noise; see the supporting information for details.

[21] In real-time prediction, the PNF algorithm for choosing noise snippets has to deal with "end effects" that bias the SSA reconstruction and the estimated value of the LFM phase at the forecast starting time. For the predictability study presented here, we computed the RC pair that captures the MJO's LFM by using the entire data record available, in order to present the optimal PNF skill as proof of concept. It is left for future research to explore ways to minimize such end effects for applications to operational forecasting.

[22] For the purpose of defining MJO forecast skill, we use the commonly adopted bivariate correlation (`corr`) and the root-mean-square error (`rmse`) between the observed and forecast RMM indices [*Gottschalck et al.*, 2010]. The skill of the PNF method is notably better than the standard EMR: See the blue versus red curves in Figure 2a. Moreover, PNF compares favorably with existing statistical and dynamical models for MJO prediction (cf. section 1).

[23] Even though PNF is applied here to RMM1 only, prediction of RMM2 is also improved, since both indices are physically coupled. The potential increase in predictability by PNF (blue) versus EMR (red) in the time domain coincides mostly with energetic phases of MJO's LFM; these phases are well captured by the leading RC pair with an SSA window of 50 days (cyan) (cf. Figure 1d). This PNF feature is due to the method's intrinsic conditioning of the driving noise on the LFM phase. On the other hand, EMR and PNF predictions are similar when LFM is weak, i.e., during March–April 2006, as seen in Figure 1d.

[24] The time series of EMR forecasts are expected to have smaller variance than the PNF ones since—at long lead times and when averaged over a large ensemble of driving-noise realizations—they converge to the climatological mean. PNF, though, picks out certain members of that ensemble that enhance LFM prediction. Moreover, averaging over the PNF ensemble aims to follow the relatively

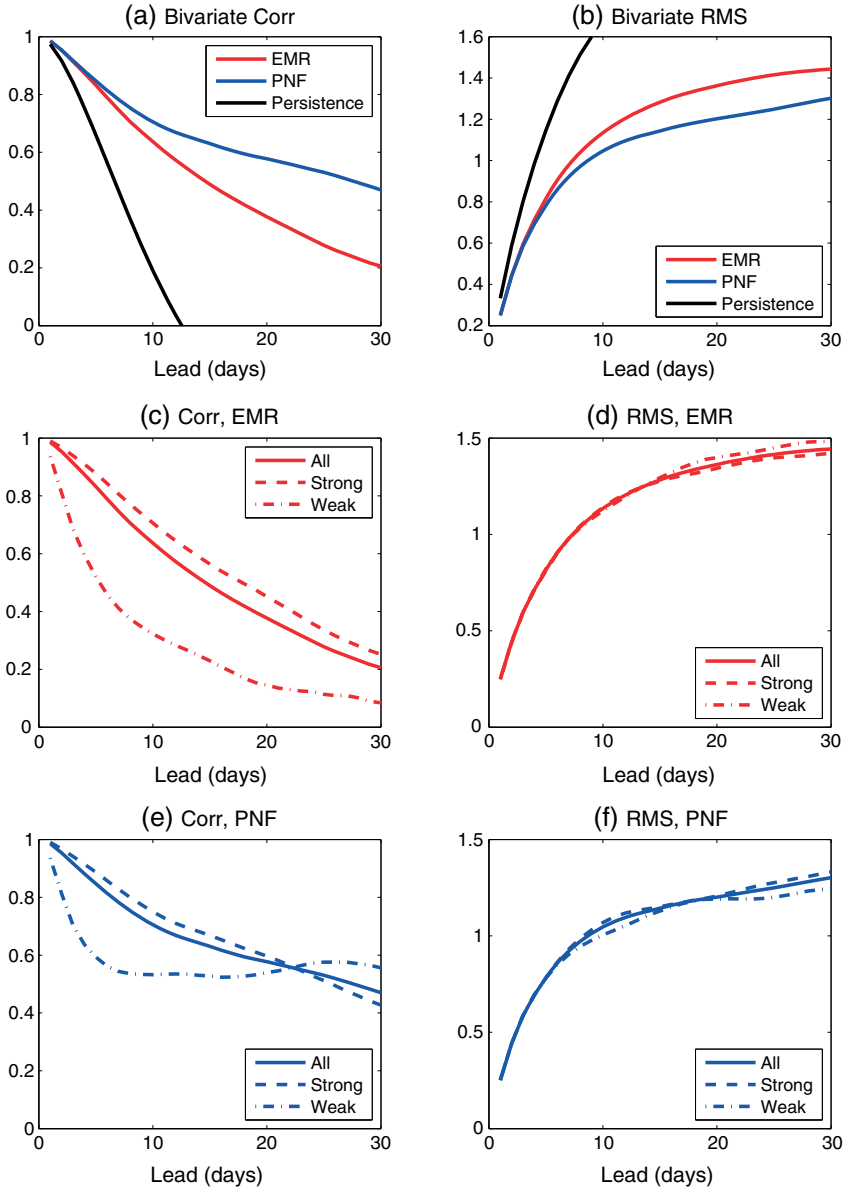


Figure 2. Skill scores for prediction by EMR alone and by EMR driven by PNF snippets. (a) Bivariate correlation (`corr`) and (b) root-mean-square error (`rmse`) between the observed and forecast RMM indices showing increase in predictability of RMM1–2 beyond 15 days by PNF (blue) versus EMR (red); the black curve shows damped persistence as a basis for comparison. (c–f) Prediction skill as a function of the MJO strength at the start of the forecast: PNF improvement is most pronounced for weak MJO, especially in correlation.

smooth LFM trajectory and, therefore, PNF improvement for `rmse` (amplitude) is less pronounced than in `corr` (phase) (see the supporting information).

[25] Figures 2c–2f compare prediction skill for the forecasts started for weak versus strong MJO events, defined as $\{(\mathrm{RMM1})^2 + (\mathrm{RMM2})^2\}^{1/2} < 1$ or ≥ 1, respectively. The `rmse` barely depends on the MJO strength for either EMR or PNF predictions (Figures 2d and 2f). Correlation skill `corr` when using EMR alone, however, is much worse for weak versus strong MJO variability (Figure 2c), while PNF improves forecasts started during strong as well as weak MJO events. It does so much more dramatically in terms of `corr` in the latter case, when it exceeds the overall mean skill (Figure 2e). PNF is thus able to better capture the growth of strong MJO events, an observation that is also consistent with improvement in the time domain (Figures 1c and 1d).

[26] Figures 3a–3d present prediction skill conditioned on the eight MJO phases (as defined by $\tan^{-1}$(RMM2/RMM1) in *Wheeler and Hendon* [2004]; cf. Figure 1c) at the start of the forecast. Physically, these phases describe different geographical locations of MJO convective activity.

[27] MJO events started in phases 3 and 8, i.e., over the Indian Ocean and tropical Africa, are best predicted; they result in forecasts with the largest `corr` and smallest `rmse`, respectively. There is also general improvement in PNF for `rmse` around phases 2–5. The decrease in `corr` for PNF predictions started during phases 4–5 corresponds to the well-known difficulties of simulating [*Vitart and Molteni*, 2010] and predicting [*Zhang and van den Dool*, 2012] MJO

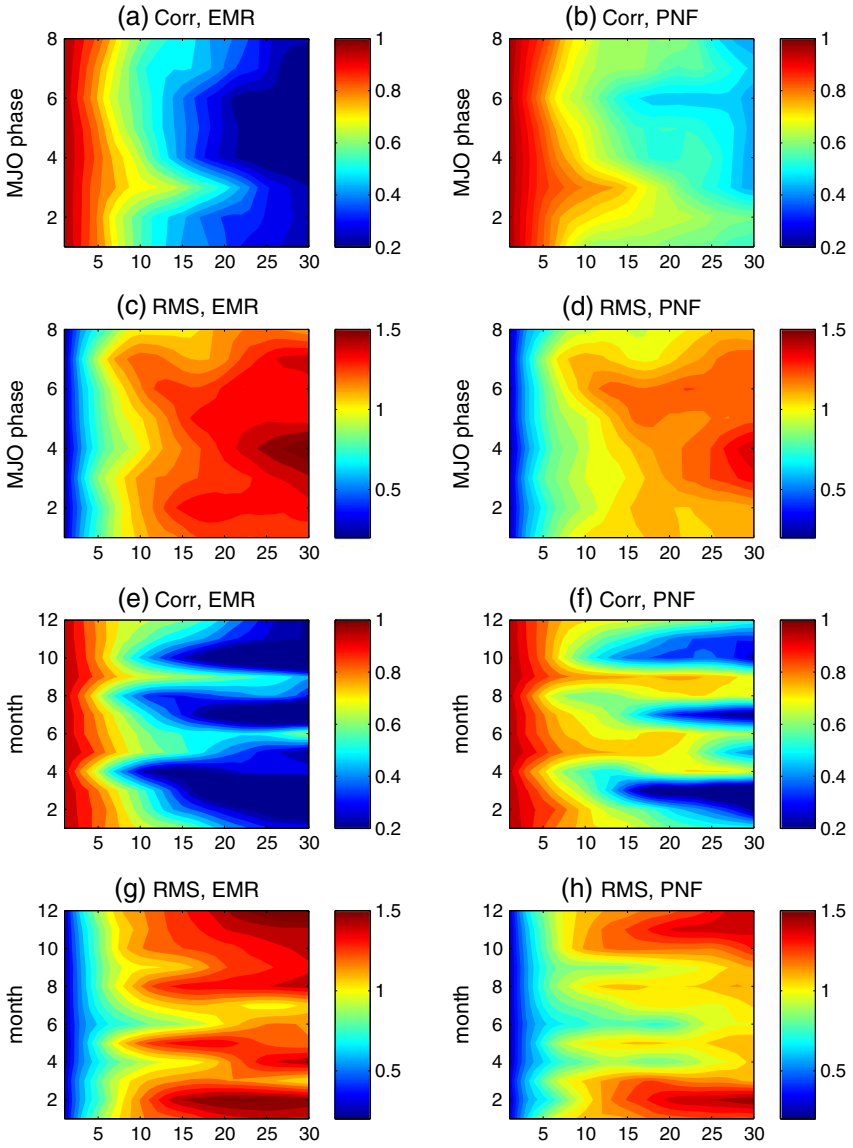


Figure 3. Prediction skill conditioned (a–d) on the phase of the MJO and (e–h) on the calendar month at the start of the forecast for EMR only and EMR driven by PNF snippets.

when it crosses the Maritime Continent. These difficulties are sometimes referred to as "the Maritime Continent prediction barrier," reminiscent of the "spring barrier" for ENSO prediction [*Barnston et al.*, 2012].

[28] Figures 3e–3h show strong seasonality in the `corr` and the `rmse`. The correlation gets higher in boreal summer and early fall, as well as during boreal winter, while the `rmse` is smallest during late summer and early fall. This result agrees with the perception that MJO is more active and better organized during certain seasons [*Ghil and Mo*, 1991; *Wheeler and Hendon*, 2004; *Zhang and van den Dool*, 2012]. Our results here show that the EMR and PNF prediction methods can capture well the mostly eastward propagating MJO in boreal winter, as well as the additional, northward propagating component in boreal summer.

4. Conclusions

[29] We presented results of a predictability study in which the EMR and PNF methodologies were applied to MJO, with the ultimate goal to use and test these methods in real-time forecasting. The bivariate forecast skill obtained by PNF, in both phase and amplitude, is useful up to 30 days and comparable with the skill demonstrated by a dynamical multimodel ensemble [*Zhang et al.*, 2013]. The PNF improvement over EMR alone is most pronounced for predictions started during weak MJO events, over Africa and the Indian Ocean, and during boreal summer and early fall.

[30] **Acknowledgments.** It is a pleasure to thank Adam Sobel and Daehyun Kim for their valuable input, and an anonymous reviewer for thoughtful and stimulating comments. This study was supported by grants NSF DMS-1049253 and NSF OCE-1243175 from the National Science Foundation, ONR-MURI N00014-12-1-0911 from the Office of Naval Research, and DOE-DE-F0A-0000411 from the Department of Energy.

[31] The Editor thanks an anonymous reviewer for assisting in the evaluation of this paper.

References

Barnston, A. G., M. K. Tippett, M. L. Heureux, S. Li, and D. G. DeWitt (2012), Skill of real-time seasonal ENSO model predictions during

2002–2011—Is our capability improving?, *Bull. Am. Meteorol. Soc.*, *93*, 631–651.

Chekroun, M., D. Kondrashov, and M. Ghil (2011a), Predicting stochastic systems by noise sampling, and application to the El Niño–Southern Oscillation, *Proc. Natl. Acad. Sci. USA.*, *108*, 11,766–11,771.

Chekroun, M. D., E. Simonnet, and M. Ghil (2011b), Stochastic climate dynamics: Random attractors and time-dependent invariant measures, *Physica D*, *240*(21), 1685–1700.

Feliks, Y., M. Ghil, and A. W. Robertson (2010), Oscillatory climate modes in the Eastern Mediterranean and their synchronization with the North Atlantic Oscillation, *J. Clim.*, *23*, 4060–4079.

Ghil, M., and K.-C. Mo (1991), Intraseasonal oscillations in the global atmosphere. Part I: Northern Hemisphere and tropics, *J. Atmos. Sci.*, *48*, 752–779.

Ghil, M., and A. W. Robertson (2002), "Waves" vs. "particles" in the atmosphere's phase space: A pathway to long-range forecasting?, *Proc. Natl. Acad. Sci. USA.*, *99*(Suppl. 1), 2493–2500.

Ghil, M., et al. (2002), Advanced spectral methods for climatic time series, *Rev. Geophys.*, *40*, 3.1–3.41, doi:10.1029/2000RG000092.

Gottschalck, J., et al. (2010), A framework for assessing operational Madden-Julian Oscillation forecasts: A CLIVAR MJO Working Group project, *Bull. Am. Meteor. Soc.*, *91*, 1247–1258.

Jiang, X., D. E. Waliser, M. C. Wheeler, C. Jones, M.-N. Lee, and S. D. Schuert (2008), Assessing the skill of an all-season statistical forecast model for the Madden-Julian Oscillation, *Mon. Wea. Rev.*, *136*, 1940–1956.

Kang, I.-S., and H.-M. Kim (2010), Assessment of MJO predictability for boreal winter with various statistical and dynamical models, *J. Clim.*, *23*, 2368–2378.

Kondrashov, D., S. Kravtsov, A. W. Robertson, and M. Ghil (2005), A hierarchy of data-based ENSO models, *J. Clim.*, *18*, 4425–4444.

Kondrashov, D., S. Kravtsov, and M. Ghil (2011), Signatures of nonlinear dynamics in an idealized atmospheric model, *J. Atmos. Sci.*, *68*, 3–12.

Kravtsov, S., D. Kondrashov, and M. Ghil (2005), Multilevel regression modeling of nonlinear processes: Derivation and applications to climatic variability, *J. Clim.*, *18*, 4404–4424.

Kravtsov, S., D. Kondrashov, and M. Ghil (2009), Empirical model reduction and the modeling hierarchy in climate dynamics, in *Stochastic Physics and Climate Modeling*, edited by T. N. Palmer and P. Williams, pp. 35–72, Cambridge Univ. Press, Cambridge.

Love, B. S., and A. J. Matthews (2009), Real-time localised forecasting of the Madden-Julian Oscillation using neural network models, *Q. J. R. Meteorol. Soc.*, *135*(643, Part b), 1471–1483.

Maharaj, E., and M. Wheeler (2005), Forecasting an index of the Madden-Julian Oscillation, *Int. J. Climatol.*, *25*, 1611–1618.

Penland, C., and P. D. Sardeshmukh (1995), The optimal growth of tropical sea surface temperature anomalies, *J. Clim.*, *8*, 1999–2024.

Seo, K.-H., W. Wang, J. Gottschalck, Q. Zhang, J.-K. E. Schemm, W. R. Higgins, and A. Kumar (2009), Evaluation of MJO forecast skill from several statistical and dynamical forecast models, *J. Clim.*, *22*, 2372–2388.

Vautard, R., and M. Ghil (1989), Singular spectrum analysis in nonlinear dynamics, with applications to paleoclimatic time series, *Physica D*, *35*, 395–424.

Vitart, F., and F. Molteni (2010), Simulation of the Madden–Julian Oscillation and its teleconnections in the ECMWF forecast system, *Q. J. R. Meteorol. Soc.*, *136*, 842–855.

Wheeler, M. C., and H. Hendon (2004), An all-season real-time multivariate MJO index: Development of an index for monitoring and prediction, *Mon. Wea. Rev.*, *132*, 1917–1932.

Wouters, J., and V. Lucarini (2013), Multi-level dynamical systems: Connecting the Ruelle Response Theory and the Mori-Zwanzig Approach, *J. Stat. Phys.*, *151*, 850–860.

Zhang, C., J. Gottschalck, E. D. Maloney, M. W. Moncrieff, F. Vitart, D. E. Waliser, B. Wang, and M. C. Wheeler (2013), Cracking the MJO nut, *Geophys. Res. Lett.*, *40*, 1223–1230, doi:10.1002/grl.50244.

Zhang, Q., and H. van den Dool (2012), Relative merit of model improvement versus availability of retrospective forecasts: The case of Climate Forecast System MJO prediction, *Weather Forecasting*, *27*, 1045–1051.